Positioning of Single Co Atoms Steered by a Self-assembled Organic Molecular Template

Wolfgang Krenner,[*,†] Florian Klappenberger,[†] Dirk Kühne,[†] Katharina Diller,[†] Zhi-Rong Qu,[‡] Mario Ruben,[‡,¶] and Johannes V. Barth[†]

Physik Department E20, Technische Universität München, James-Franck Straße, 85748 Garching, Germany, and Institute of Nanotechnology, Karlsruhe Institute of Technology, 76021 Karlsruhe, Germany

E-mail: wkrenner@ph.tum.de

Phone: +49 89 12848. Fax: +49 89 12338

Abstract

The bonding and organization of cobalt atoms on a self-assembled organic molecular template are investigated by low-temperature scanning tunneling microscopy. In a first step, N,N'-diphenyl oxalic amide is deposited on the Ag(111) surface with sub-monolayer and monolayer coverage leading to the formation of supramolecular nanogratings and a dense-packed layer, respectively. These templates are exposed to evaporated cobalt at different substrate temperatures in the range of 110 to 240 K. We find that Co always binds on top of the phenyl rings, thus the realization of Co-phenyl complexes is preferred over metal cluster growth on the bare Ag(111) surface. In the case of the dense-packed template a large fraction of the provided Co is engaged in the formation of well-defined, uniform monomeric Co-half-sandwich structures.

[*]To whom correspondence should be addressed

[†]Physik-Department E20, Technische Universität München

[‡]Institute of Nanotechnology, Karlsruhe Institute of Technology (KIT)

[¶]IPCMS-CNRS UMR 7504, Université de Strasbourg, 23 Rue du Loess, 67034 Strasbourg (France)

At an optimal growth temperature of 180 - 200 K the fraction of monomeric Co species on the template exceeds 80% of the total amount of Co deposited. The temperature-dependent adsorption behavior and monomer fraction are compared to calculations, simulating the growth process in the diffusionless limit by a hit-and-stick adsorption model. This analysis indicates that the organic template suppresses the clustering tendency inherent to diffusing Co atoms and allows the production of a monomer fraction as high as that for statistical growth in the low coverage regime.

TOC Graphic

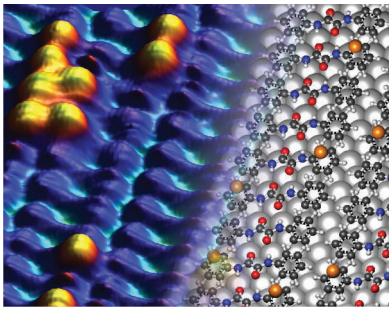

Keywords: STM, Self-Assembly, Organic Molecules, Cobalt, Single Atoms

Single atoms on surfaces are possible units for future high-density magnetic data storage or spin computation applications. Therefore, in recent years the organization and magnetic properties of single spin species have been under extensive investigation.[1–7] Experiments have shown that the magnetic anisotropy energy, which leads to an alignment of the magnetization along specific spatial directions rather than randomly oscillating spins, depends strongly on the exact dimensionality, arrangement and substrate used in these systems.[8–15] Furthermore, the interaction between these spins gives rise to intriguing phenomena like the many-body Kondo effect and magnetocrystalline anisotropy.[14–17] Extensive research towards ordered arrays of single molecule magnets and their properties has also shown to provide a possible route towards the realization of molecular spintronics.[18–22] As a whole, the field of research towards single magnetic species is limited by the level of control over the creation of magnetic objects. Thus, for the realization of future mag-

netic nanodevices, the development of novel techniques to steer the formation of low-dimensional magnetic systems is a necessary prerequisite.

Recently structures formed by bonding of Co dimers on benzene or graphene have been predicted to show huge magnetic anisotropies and were therefore proposed as candidates for magnetic storage applications.[23–25] To study the route towards the realization of these structures, in this work we employed a supramolecular engineering approach[26] to produce arrays of single magnetic atoms on top of a molecular template. Specifically, we used low-temperature scanning tunneling microscopy (STM) to investigate, first, the self-assembly N,N'-diphenyl oxalic amide molecules[27–29] on the Ag(111) surface and, second, the organization and bonding of Co atoms on the templated surface. The organic precursor forms, depending on coverage, nanogratings or a perfect dense-packed monolayer, on which Co adsorbs on top of the phenyl rings yielding Co-half-sandwich complexes,[30–32] i. e., complexes with a single magnetic metal atom and Co clusters. In the saturated organic layer case, the adsorption behavior depends on the substrate temperature during growth and the cobalt coverage, yielding high amounts of Co monomers. A comparison to the cluster distribution predicted for diffusionless growth by a simple statistical adsorption theory assuming a hit-and-stick behavior shows that the template is suppressing Co diffusion and cluster formation.

In the experiments we prepared templates of organic N,N'-diphenyl oxalic amide molecules (see Figure 1a) constructed *via* self-assembly. For molecule coverages below one monolayer (ML) an arrangement of approximately equally spaced lines of molecules (appearing brighter than the substrate) is observed (see Figure 1b), similar to supramolecular gratings reported earlier.[33–35] Pairs of molecules forming a substructure in the chains are encountered (see Figure 1c). An angle of $\alpha \simeq 70^\circ$ between the direction of the molecular nanowires and the long axis of molecules themselves as well as a slight tilt of the phenyl moiety with respect to the surface plane is observed in this case.[28,29] However, recent theoretical work indicates a different bonding scheme as proposed in references 28 and 29 for stabilizing the chain formation, which will be discussed in an upcoming publication.

Cobalt evaporation onto such a sample held at a deposition temperature (T_{dep}) of 130 K leads to a decoration of the molecules appearing as white dots on gray molecules, whereas no adsorption on the silver surface (black) is observed (see Figure 1d). For comparison, evaporation of Co onto the pristine surface without the organic template under similar conditions leads to the formation of clusters with a lateral size of several nanometers prevalently attached to the step edges.[36] Thus, in our case the presence of the molecular nanostructure suppresses the growth of large clusters and drastically reduces the size of the Co formations. The smallest objects are in the sub-nm regime and situated on either side of the nanowires, but not in the center. However, there are also large clusters, frequently connected with breaking and bending of the molecular lines (see Figure 1d). The limited stability of the nanowires hence prevents the expression of regular nanostructures. By contrast, it was recently demonstrated by Decker *et al.*,[37] that with a more stable template, namely a self-assembled metal-organic network constructed from dicarbonitrile-polyphenyl coordinated to Co centers,[38,39] it is possible to create metal clusters on top of the template without destroying the molecular layer.

For a coverage of a saturated ML a dense-packed arrangement of the molecules is observed (see Figure 2a). Even after evaporation of a sufficient amount of molecules onto a sample held at room temperature no multilayer formation occurred. We conclude that excess molecules desorb again under these conditions. Therefore, a perfect dense-packed monolayer covering the entire surface can easily be constructed. In this case the supramolecular structure differs from the submonolayer (sub-ML) case because no pairing occurs within the entire domain. The angle β between the nanowire direction and the molecular backbone amounts to $\beta \simeq 80^\circ$ (see Figure 2b). The packing theme resembles the structure also found in the bulk crystal.[29]

When Co is deposited onto the organic ML, sub-nm sized structures evolve in a highly site-selective process, again. As evidenced in the high-resolution image in Figure 2c, the Co-induced nanostructures feature uniform structural characteristics. They are imaged as circular dots with an apparent diameter of ~ 6 Å and an apparent height below 1 Å, with the exact height depending on the experimental conditions, mainly the state of the tip and the bias voltage. Co atoms are

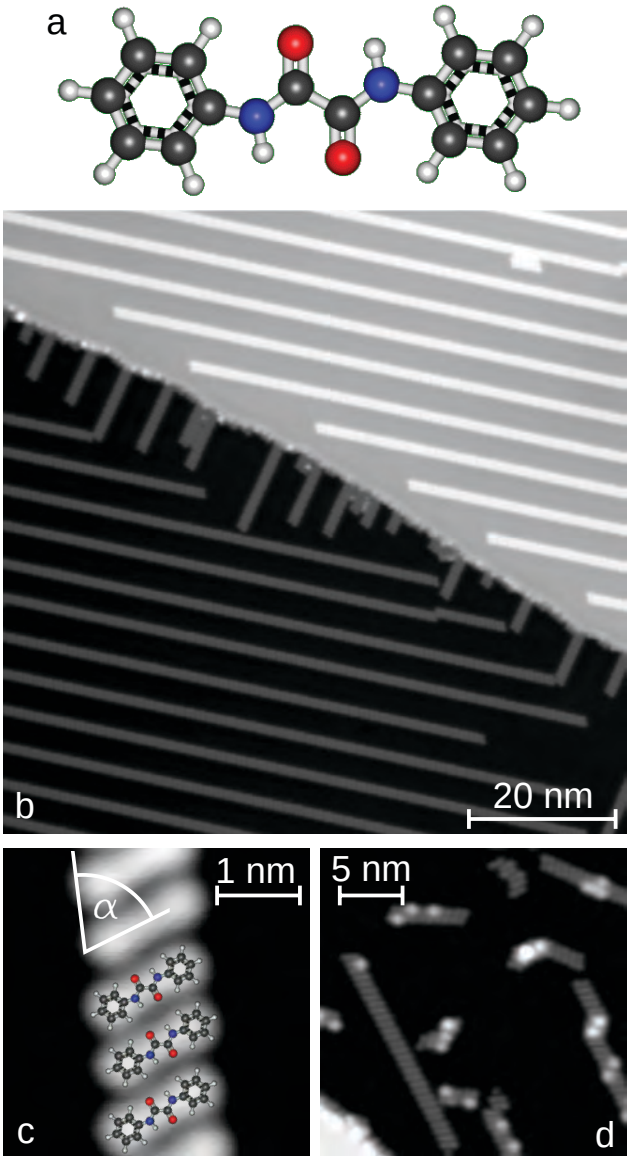

Figure 1: (a) Structure model of N,N'-diphenyl oxalic amide (H white, C black, O red, N blue). (b) Overview image of equally spaced molecular lines assembled on the Ag(111) surface. (Bias voltage V_B = -1.0 V, tunneling current I_T = 0.1 nA) (c) High resolution image with molecular models superimposed. (V_B = -0.3 V, I_T = 0.11 nA) A single molecule is imaged as a dog-bone like protrusion. This appearance originates from the two broader phenyl rings at the outer ends connected by a thinner waist. An arrangement of molecules forming pairs as a substructure of the nanowires is observed. This leads to $\alpha \simeq 70^\circ$ between the nanowire direction and the molecular backbone. (d) Addition of Co at low temperatures (T_{dep}=130 K) leads to adsorption on top of the phenyl rings instead of adsorbing to the silver surface. However, lines start to bend and break when Co is present. (V_B = -0.2 V, I_T = 0.1 nA)

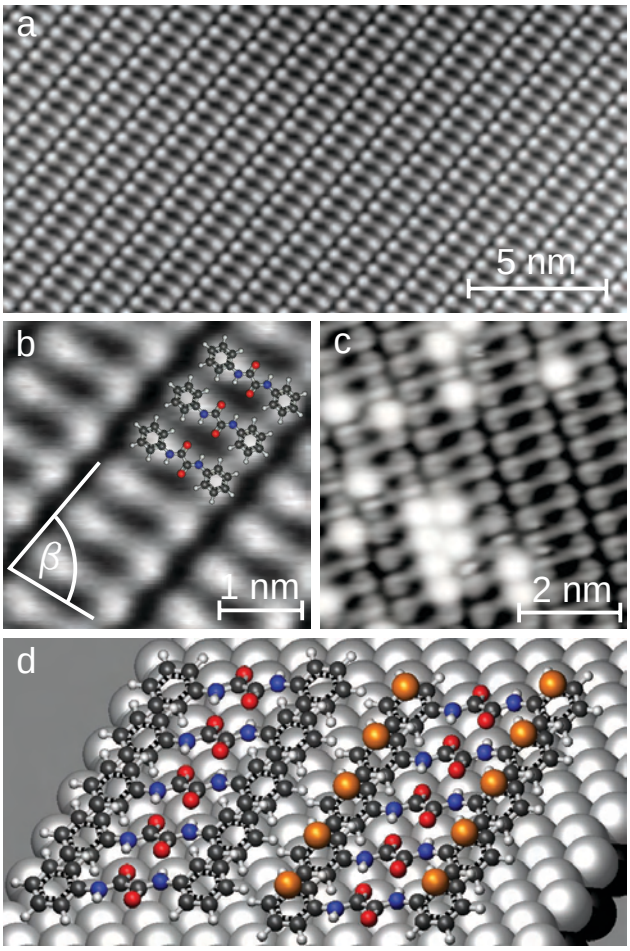

Figure 2: (a) Topographic image of a dense-packed ML of N,N'-diphenyl oxalic amides. (V_B = -1.25 V, I_T = 0.06 nA) (b) High resolution image with superimposed molecular model highlights the bonding scheme. (V_B = -0.31 V, I_T = 0.1 nA) The molecules form two hydrogen bonds with each adjacent molecule, which leads to a bulk-like arrangement with $\beta \simeq 80°$. (c) Co atoms (bright protrusions) adsorb monomerically on top of the phenyl rings of the molecules without inducing defects in the organic template. (V_B = -0.98 V, I_T = 0.09 nA) (d) 3D visualization of bare molecules (left row) and molecules with Co (orange) adsorbed on top (right row) in the ideal case of all phenyl rings being occupied by a single atom, thereby forming a dense-packed arrangement on the Ag(111) surface (silver spheres underneath).

positioned at the phenyl ring positions of the molecules. From the uniform shape and small size we conclude, that each dot actually represents a single Co atom. This interpretation is consistent with the amount of Co expected on the basis of the flux calibration of the evaporator used in the experiments. The unoccupied part of a molecule hosting a Co atom is imaged with the same characteristics as the corresponding part of a molecule without Co attached. This observation indicates, that the Co is residing on top of the phenyl ring. For the case of a Co atom positioned between the phenyl moiety and the Ag substrate, an uplift of the molecule would result, entailing a change in the appearance of the molecule. Therefore, we conclude that uniform Co-half-sandwich structures[30–32] are formed.

In contrast to the sub-ML grating the saturated organic layer is stable enough to host high Co densities without a modification of its structure. This can be attributed to the high packing density increasing the stability due to more lateral intermolecular interaction in contrast to the sub-ML regime.

However, defect and cluster formation cannot be eliminated completely. As shown in Figure 3a, the major part of the Co adsorbs monoatomically (imaged as yellow dots residing on the molecular template depicted as orange, dog-bone like protrusions), whereas defects, i.e., clusters with more than one atom, appear as white regions with irregular shape and height.

A high-resolution image (Figure 3b) is used to exemplify the following analysis of cluster sizes based on their apparent height. The upper linescan across a line of monomers (blue) shows a maximal variation of the apparent height of atoms adsorbed along the phenyl ring chain of adjacent molecules of only 0.2 Å (Figure 3c, upper panel). The lower linescan across two monomers and a cluster (Figure 3b, red) displays an apparent height difference of $\sim$0.6 Å, which can be clearly distinguished from the variations of the monomers. Clusters with characteristics as defined by the red linescan are assumed to consist of two Co atoms probably stacked upwards on one another. Such a stacking was already demonstrated on the bare Ag(111) surface for Mn atoms by Kliewer *et al.*[40] So in the samples prepared in our approach Co-dimers as proposed by Xiao, *et al.*[23,24] and Cao, *et al.*[25] are formed only as rare events. However, with increasing coverage higher concentrations of

Co-dimers may become more likely to be formed. As is explained in the SI in further detail, we approximated larger clusters to be cone-shaped structures of several layers of Co stacking upwards on several monomers adsorbed on neighboring phenyl rings.

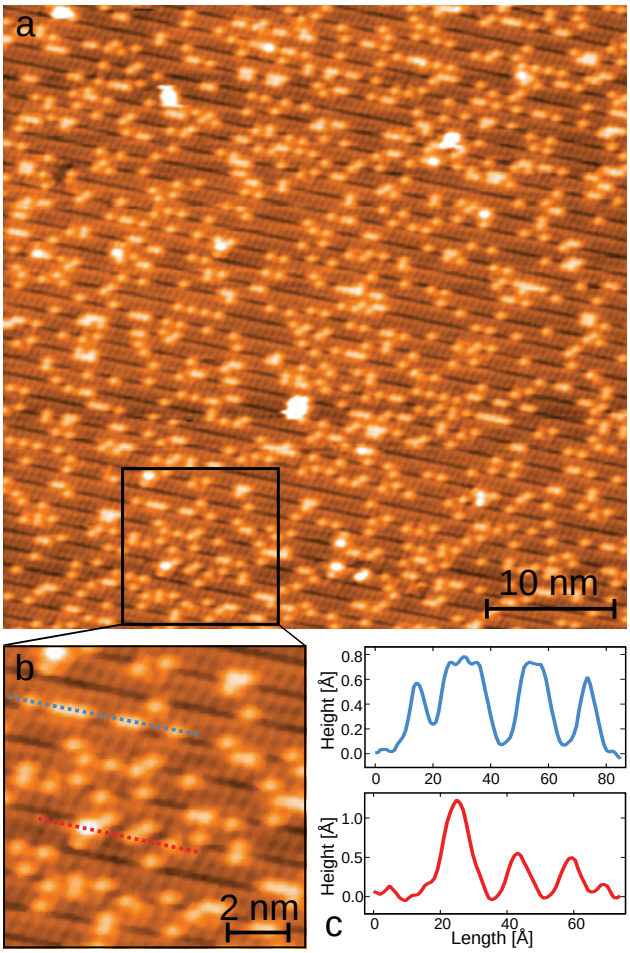

Figure 3: (a) Overview image of Co atoms adsorbed on the dense-packed ML (125 s Co at a flux of 0.0018 MLs/s, T_{dep}=180 K, V_B = 1.0 V, I_T = 0.1 nA). Co monomers appear as yellow protrusions, whereas defects are imaged as white protrusions on the orange molecular template. In a zoomed in area of the sample (b) an enhancement in the apparent height (∼30%, from ∼0.6 Å to ∼0.8 Å) for adatoms adsorbed on neighboring phenyl rings (blue dashed line) can be distinguished from the enhancement (∼100%, from ∼0.6 Å to ∼1.2 Å) due to the presence of a dimer (red dashed line) as can be seen in the corresponding line scans (c).

With these assumptions, we examined the ratio between monoatomic Co adsorbates and defects in dependence of the substrate temperature during Co deposition (Figure 4). A series of experiments was carried out, wherein the total evaporated amount of Co was kept constant, while the sample temperature during metal evaporation was varied from 110 to 240 K. The nominal

amount of Co was chosen to cover ∼23% of the phenyl rings provided by the template if all Co atoms were adsorbed monoatomically. Thus, the samples had a Co coverage of 0.23 MLs, defining a ML as one Co atom per phenyl ring of the template. For low temperatures, starting at 110 K (Figure 4a), a substantial amount of the deposited Co atoms is found to form clusters (irregular, white protrusions) instead of to single atoms (yellow dots). The fraction of monoatomic Co of the total amount of deposited metal atoms, from here on referenced to as monomer fraction (MF), is determined to be ∼50%. In this fraction the total Co amount is the nominal amount calculated from the flux calibration and the evaporation time. With increasing sample temperature, the MF increases (Figure 4d) until a maximum is reached at T_{dep}=190 K. An image recorded on a sample grown at T_{dep}=190 K (Figure 4b) demonstrates that the majority of adsorbates appear as circular and uniform protrusions, whereas defects show a tendency towards increased size, but clearly form less frequently. Under these optimal growth conditions the MF peaks at ∼80%. For temperatures exceeding 200 K cluster formation increases, therefore the MF declines. As shown for 240 K in Figure 4c, the number of single atoms (yellow protrusions) is strongly reduced, whereas the formation of clusters with rather similar shape and size (bright protrusions) is encountered, with the MF being reduced to ∼45%. The dependence of the MF on T_{dep} is displayed in Figure 4d, where the value for all samples of the series are given with blue dots. The curve exhibits a maximum at an optimal temperature T_{opt} = 190 K. With increasing temperature difference to T_{opt} the MF decreases monotonically to lower as well as to higher temperatures. This behavior suggests two competing effects which govern the growth process. Based on the comparison with the model value we suggest the following scenario to govern the MF dependence. The MF at low temperature ($T_{dep} < T_{opt}$) is significantly less than the expectation value calculated in the hit-and-stick model. This difference indicates that Co atoms undergo transient motion after their impact on the organic layer until the non-equilibrium adsorption energy is dissipated. Meta-stable clusters are formed during this process. With increasing T_{dep} these cluster are increasingly dissolved by the equilibrium thermal excitation during the time of evaporation. At T_{opt} the diffusion of the Co monomers is still small if not negligible and thus the model MF is reached. In the high-temperature regime

($T_{dep} > T_{opt}$), diffusion of the adatoms becomes increasingly important and allows the formation of larger clusters which are stable at these temperatures and to which the monomers aggregate.

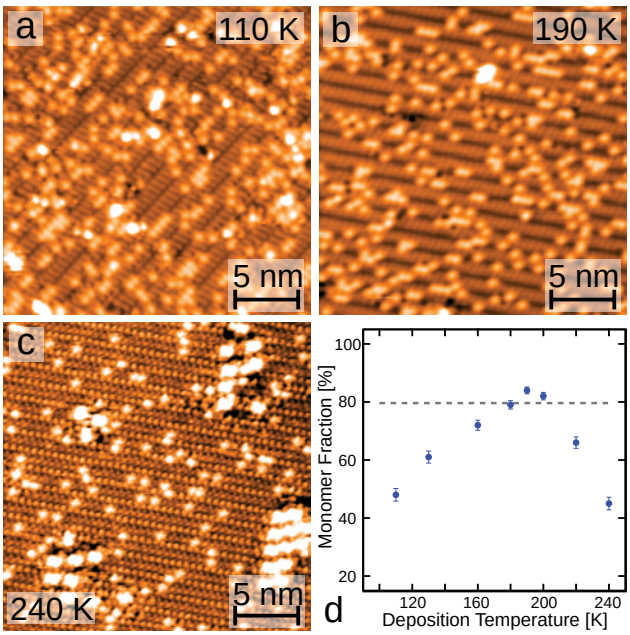

Figure 4: Exemplary topographs of samples with a constant Co coverage (0.23 MLs) evaporated at varying deposition temperatures (T_{dep} as indicated) onto the dense-packed organic template and monomer fraction analysis for the complete series of experiments. (a) At T_{dep}=110 K Co monomers (yellow) and numerous defects of different size (white) cover the organic template (dark orange). (V_B = 0.6 V, I_T = 0.05 nA) (b) At ideal growth conditions (T_{dep} = 190 K) monomeric Co dominates over a small number of defects which are characterized by a larger average size than in the previous case. (V_B = 0.4 V, I_T = 0.08 nA) (c) For T_{dep} = 240 K the number of monomers is smaller and the defects are larger than for lower temperatures. The defects have a tendency towards a distinct, uniform shape. (V_B = 0.9 V, I_T = 0.1 nA) (a-c) Note that the change in the appearance of the molecular template is due to different imaging conditions and not due to a change in the molecular layer. (d) The monomer fraction is small (∼40%) at both ends of the studied temperature range and increases monotonically towards the optimal growth temperature (T_{dep} = 190 K). The gray dashed line indicates the value expected for such a coverage from a simple hit-and-stick statistics. Under ideal growth conditions this value is nominally slightly exceeded.

After optimizing the growth temperature, a series of samples was prepared with increasing Co coverage at T_{dep} = 180 K. The coverage was increased in three steps from 125 s deposition time, corresponding to 0.23 ML of Co, to 510 s, corresponding to 0.91 ML of Co. Exemplary topographs from this series of experiments are shown in Figure 5a-c. In Figure 5a the majority of Co atoms adsorb as single species (yellow protrusions on orange molecular template), whereas the amount of defects (brighter protrusions) is comparably low. With increasing Co coverage (Figure 5b) the

amount of monomers increases as well as the density of defects. At high Co density (0.91 ML in Figure 5c) it becomes difficult to make a clear distinction between monomers and defects. The result of a statistical analysis of the MF for the four coverages 0.23, 0.34, 0.47 (topograph not shown) and 0.91 MLs is reproduced in Figure 5d (blue dots). With increasing Co coverage the MF decreases monotonically.

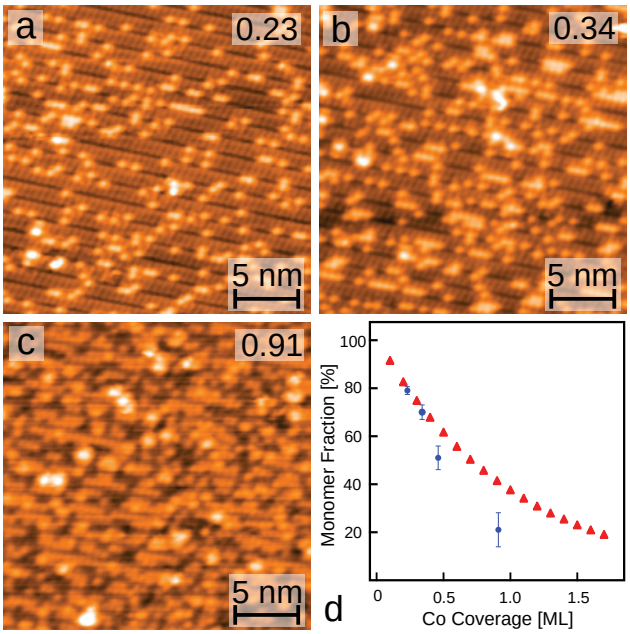

Figure 5: (a)-(c) Overview topographs of samples with increasing Co coverage and constant T_{dep} = 180 K. The fraction of a ML is indicated in the upper right corner of each image. With increasing coverage an increase of Co atoms arranged in linear chains is observed (V_B = 1.0 V, I_T = 0.1 nA for all). (d) The MF decreases with increasing coverage (blue dots, Co flux of 0.0018 MLs/s during deposition). The calculations (red triangles) following a hit-and-stick adsorption in the diffusionless limit show a deviation from experimental values (blue dots) for Co coverages exceeding ∼0.4 MLs. This observation is attributed to enhanced interatomic interactions that influence the Co distribution at high coverages.

To gain further insight into the growth process, we simulated the distribution of atomic Co on the molecular precursor following a strict hit-and-stick process. In these calculations we assumed that adsorbates do not perform any diffusion steps across the molecular precursor, but rather directly stick to the first adsorption site encountered upon impact. As adsorption site the area of a phenyl ring is taken into account and sticking to this site is possible no matter whether the phenyl ring is still free or already occupied by a previous Co atom. In the model the adsorption sites cover

the full surface, i. e., Co atoms hitting the amide moiety of the organic precursor are counted to the nearest adsorption place. By assuming a random statistical distribution for hitting the different adsorption sites, an expectation value for the MF was calculated (for details, see SI). As shown in Figure 4d the expected value for the MF from this simulation is $\sim$79% (gray dashed line) for a coverage of 0.23 MLs of Co. The evolution of the MF depending on the Co coverage at 180 K is compared to the respective expectation values in Figure 5d.

Comparing the experimental results of the MF in dependence of the coverage to the statistical hit-and-stick analysis, it is found that for coverages up to 0.34 MLs the experimental MF is in good agreement with numerical predictions. However, for higher coverages the fraction of Co monomers falls below the predicted value. This discrepancy is consistent with our hypothesis that the formation of stable clusters depends on the statistic probability of Co collision events, which in turn increases with coverage at identical temperatures.

In conclusion, we demonstrated a novel approach towards the construction of arrays of single magnetic atoms. Co atoms were adsorbed on top of phenyl rings, provided by an organic template, namely a dense-packed layer of N,N'-diphenyl oxalic amides, and form monoatomic Co-half-sandwich complexes and multiatomic Co clusters with relative amounts of each depending on the sample temperature during evaporation. The deposition conditions were optimized in order to increase monomeric adsorption. The optimal temperature of the substrate was found to be in the range of 180 - 200 K. The complex behavior of the monomer fraction is interpreted to be a result of two counteracting effects, namely stabilization of metastable small clusters at low temperatures and the statistic formation of stable large clusters at high temperatures.

The realized half-sandwich compounds bear interesting aspects for surface-confined metallo-supramolecular chemistry.[41,42] They notably represent potential templates to create surface analogons to bis(benzene) organometallic sandwich complexes. In a similar way we recently realized cerium-porphyrinato species by assembly and synthesis protocols on well-defined metal surfaces.[43] Employing an organic molecular template anchored on a surface may therefore prove to be a feasible route towards the construction of novel magnetic storage devices as proposed recently

by theory.[23–25]

Our work demonstrates the possibility of creating hybrid organometallic surface nanoarchitectures constructed from single atoms using an organic molecular precursor, which acts as an ordered template for atomic organization. Structures constructed in this fashion may open up new possibilities for the realization of novel nanomagnetic or spintronic concepts, whereby single atoms and their spins act as smallest functional units.

Methods

All sample preparations and experiments were carried out in an UHV apparatus with a base pressure of less than 10^{-10} mbar. The Ag(111) surface was prepared by repeated Ar^{+} bombardment at an energy of 1 keV followed by annealing to 750 K for $\sim$10 min. The investigated molecular templates were formed by OMBE of N,N'-diphenyl oxalic amide molecules[27] from a quartz crucible, which was heated in a Knudsen cell held at $\sim$417 K onto the Ag substrate held at room temperature (297 K). Thereafter, the samples were cooled down to temperatures in the range of 110 to 240 K for Co deposition from an electron beam evaporator. After metal deposition the sample temperature was held at growth temperature for several minutes, before the samples were transferred into the home-built STM,[44] where data was recorded at $\sim$14 K. In the STM images, molecules and Co adsorbates appear as protrusions and are visualized with bright colors as accordingly described in the text.

Acknowledgement

Funding by the European Union *via* ERC Advanced Grant MolArt (°247299) and the German Research Foundation (DFG) through the TUM International Graduate School of Science and Engineering (IGSSE) and TUM Institute of Advanced Study (IAS) are gratefully acknowledged.

Supporting Information Available

More detailed information on the statistical analysis of the Co monomer concentration. Explanation of hit-and-stick modeling for statistical analysis. This material is available free of charge via the Internet at `http://pubs.acs.org`.

References

(1) Barth, J. V.; Costantini, G.; Kern, K. *Nature* **2005**, *437*, 671–679.

(2) Iacovita, C.; Rastei, M. V.; Heinrich, B. W.; Brumme, T.; Kortus, J.; Limot, L.; Bucher, J. P. *Phys. Rev. Lett.* **2008**, *101*, 116602.

(3) Meier, F.; Zhou, L.; Wiebe, J.; Wiesendanger, R. *Science* **2008**, *320*, 82–86.

(4) Schiffrin, A.; Reichert, J.; Auwärter, W.; Jahnz, G.; Pennec, Y.; Weber-Bargioni, A.; Stepanyuk, V. S.; Niebergall, L.; Bruno, P.; Barth, J. V. *Phys. Rev. B* **2008**, *78*, 035424.

(5) Serrate, D.; Ferriani, P.; Yoshida, Y.; Hla, S.-W.; Menzel, M.; von Bergmann, K.; Heinze, S.; Kubetzka, A.; Wiesendanger, R. *Nat. Nanotechnol.* **2010**, *5*, 350–353.

(6) Jerratsch, J.-F.; Nilius, N.; Topwal, D.; Martinez, U.; Giordano, L.; Pacchioni, G.; Freund, H.-J. *ACS Nano* **2010**, *4*, 863–868.

(7) Enders, A.; Skomski, R.; Honolka, J. *J. Phys.: Condens. Matter* **2010**, *22*, 433001.

(8) Gambardella, P.; Blanc, M.; Brune, H.; Kuhnke, K.; Kern, K. *Phys. Rev. B* **2000**, *61*, 2254.

(9) Gambardella, P. et al. *Nat. Mater.* **2009**, *8*, 189–193.

(10) Wende, H. et al. *Nat. Mater.* **2007**, *6*, 516–520.

(11) Gambardella, P.; Rusponi, S.; Veronese, M.; Dhesi, S. S.; Grazioli, C.; Dallmeyer, A.; Cabria, I.; Zeller, R.; Dederichs, P. H.; Kern, K.; Carbone, C.; Brune, H. *Science* **2003**, *300*, 1130–1133.

(12) Weiss, N.; Cren, T.; Epple, M.; Rusponi, S.; Baudot, G.; Rohart, S.; Tejeda, A.; Repain, V.; Rousset, S.; Ohresser, P.; Scheurer, F.; Bencok, P.; Brune, H. *Phys. Rev. Lett.* **2005**, *95*, 157204.

(13) Pick, S.; Stepanyuk, V. S.; Klavsyuk, A. L.; Niebergall, L.; Hergert, W.; Kirschner, J.; Bruno, P. *Phys. Rev. B* **2004**, *70*, 224419.

(14) Hirjibehedin, C. F.; Lutz, C. P.; Heinrich, A. J. *Science* **2006**, *312*, 1021–1024.

(15) Wahl, P.; Simon, P.; Diekhoner, L.; Stepanyuk, V. S.; Bruno, P.; Schneider, M. A.; Kern, K. *Phys. Rev. Lett.* **2007**, *98*, 056601.

(16) Li, J. T.; Schneider, W. D.; Berndt, R.; Delley, B. *Phys. Rev. Lett.* **1998**, *80*, 2893–2896.

(17) Madhavan, V.; Chen, W.; Jamneala, T.; Crommie, M. F.; Wingreen, N. S. *Science* **1998**, *280*, 567–569.

(18) Mannini, M.; Pineider, F.; Danieli, C.; Totti, F.; Sorace, L.; Sainctavit, P.; Arrio, M.-A.; Otero, E.; Joly, L.; Cezar, J. C.; Cornia, A.; Sessoli, R. *Nature* **2010**, *468*, 417–421.

(19) Mannini, M.; Pineider, F.; Sainctavit, P.; Danieli, C.; Otero, E.; Sciancalepore, C.; Talarico, A. M.; Arrio, M.-A.; Cornia, A.; Gatteschi, D.; Sessoli, R. *Nat. Mater.* **2009**, *8*, 194–197.

(20) Gatteschi, D.; Cornia, A.; Mannini, M.; Sessoli, R. *Inorganic Chemistry* **2009**, *48*, 3408–3419.

(21) Bogani, L.; Wernsdorfer, W. *Nat Mater* **2008**, *7*, 179–186.

(22) Rocha, A. R.; Garcia-suarez, V. M.; Bailey, S. W.; Lambert, C. J.; Ferrer, J.; Sanvito, S. *Nat. Mater.* **2005**, *4*, 335–339.

(23) Xiao, R.; Fritsch, D.; Kuz'min, M. D.; Koepernik, K.; Eschrig, H.; Richter, M.; Vietze, K.; Seifert, G. *Phys. Rev. Lett.* **2009**, *103*, 187201.

(24) Xiao, R.; Fritsch, D.; Kuz'min, M. D.; Koepernik, K.; Richter, M.; Vietze, K.; Seifert, G. *Phys. Rev. B* **2010**, *82*, 205125.

(25) Cao, C.; Wu, M.; Jiang, J.; Cheng, H.-P. *Phys. Rev. B* **2010**, *81*, 205424.

(26) Barth, J. V. *Annu. Rev. Phys. Chem.* **2007**, *58*, 375–407.

(27) Meyer, R.; Seeliger, A. *Chem. Ber.* **1896**, *29*, 2640–2645.

(28) Klappenberger, F.; Cañas-Ventura, M. E.; Clair, S.; Pons, S.; Schlickum, U.; Qu, Z. R.; Brune, H.; Kern, K.; Strunskus, T.; Wöll, C.; Comisso, A.; De Vita, A.; Ruben, M.; Barth, J. V. *ChemPhysChem* **2007**, *8*, 1782–1786.

(29) Klappenberger, F.; Cañas-Ventura, M. E.; Clair, S.; Pons, S.; Schlickum, U.; Qu, Z. R.; Strunskus, T.; Comisso, A.; Wöll, C.; Brune, H.; Kern, K.; DeVita, A.; Ruben, M.; Barth, J. V. *ChemPhysChem* **2008**, *9*, 2522–2530.

(30) Zhang, X. Y.; Wang, J. L. *J. Phys. Chem. A* **2008**, *112*, 296–304.

(31) Pandey, R.; Rao, B. K.; Jena, P.; Blanco, M. A. *J. Am. Chem. Soc.* **2001**, *123*, 3799–3808.

(32) Pandey, R.; Rao, B. K.; Jena, P.; Newsam, J. M. *Chem. Phys. Lett.* **2000**, *321*, 142–150.

(33) Barth, J. V.; Weckesser, J.; Cai, C.; Günter, P.; Bürgi, L.; Jeandupeux, O.; Kern, K. *Angew. Chem. Int. Ed.* **2000**, *39*, 1230–1234.

(34) Schiffrin, A.; Riemann, A.; Auwärter, W.; Pennec, Y.; Weber-Bargioni, A.; Cvetko, D.; Cossaro, A.; Morgante, A.; Barth, J. V. *Proc. Natl. Acad. Sci. U. S. A.* **2007**, *104*, 5279–5284.

(35) Pennec, Y.; Auwärter, W.; Schiffrin, A.; Weber-Bargioni, A.; Riemann, A.; Barth, J. V. *Nat. Nanotechnol.* **2007**, *2*, 99–103.

(36) Morgenstern, K.; Kibsgaard, J.; Lauritsen, J. V.; Laegsgaard, E.; Besenbacher, F. *Surf. Sci.* **2007**, *601*, 1967–1972.

(37) Decker, R.; Schlickum, U.; Klappenberger, F.; Zoppellaro, G.; Klyatskaya, S.; Ruben, M.; Barth, J. V.; Brune, H. *Appl. Phys. Lett.* **2008**, *93*, 243102–1–3.

(38) Schlickum, U.; Decker, R.; Klappenberger, F.; Zoppellaro, G.; Klyatskaya, S.; Ruben, M.; Silanes, I.; Arnau, A.; Kern, K.; Brune, H.; Barth, J. V. *Nano Lett.* **2007**, *7*, 3813–3817.

(39) Kühne, D.; Klappenberger, F.; Decker, R.; Schlickum, U.; Brune, H.; Klyatskaya, S.; Ruben, M.; Barth, J. V. *J. Am. Chem. Soc.* **2009**, *131*, 3881–3883.

(40) Kliewer, J.; Berndt, R.; Minár, J.; Ebert, H. *Applied Physics A: Materials Science & Processing* **2006**, *82*, 63–66.

(41) Barth, J. V. *Surface Science* **2009**, *603*, 1533 – 1541, Special Issue of Surface Science dedicated to Prof. Dr. Dr. h.c. mult. Gerhard Ertl, Nobel-Laureate in Chemistry 2007.

(42) Lin, N.; Stepanow, S.; Ruben, M.; Barth, J. V. *Top. Curr. Chem.* **2009**, *287*, 1–44.

(43) Écija, D.; Auwärter, W.; Vijayaraghavan, S.; Seufert, K.; Bischoff, F.; Tashiro, K.; Barth, J. V. *Angew. Chem. Int. Ed.* **2011**, *50*, 3872–3877.

(44) Clair, S. Ph.D. thesis, Ecole Polytechnique Federale de Lausanne, 2004.